Design and analysis of high-speed coreless axial flux permanent magnet generator with circular magnets and coils

W. Fei P.C.K. Luk K. Jinupun

Department of Engineering Systems and Management, Cranfield University, Shrivenham SN6 8LA, UK
E-mail: w.fei@cranfield.ac.uk

Abstract: A high-speed coreless surface mounted axial flux permanent magnet generator with circular magnets and coils is proposed and studied. The performances of the machine are estimated and optimised by approximate theoretical analysis and comprehensive three-dimensional (3D) electromagnetic finite element analysis (FEA). Mechanical stresses in the rotor disc developed at high rotational speed are analysed and evaluated by 3D mechanical FEA to ensure the rotor's integrity. Finally, a prototype machine is constructed and tested. Both the experimental and predicted results have shown that the proposed generator possesses distinct advantages such as simple structure and high efficiency. The prototype also demonstrates its utility as a very low-cost generator.

1 Introduction

Nowadays, there are increasing interests in high-speed permanent magnet (PM) generators because of their compactness, high efficiency, reliability and self-excited feature. These desirable merits have recently captured a new range of applications, including man-portable generators and mobile battery recharge, and mission-critical energy platforms [1]. The axial flux configuration of the PM generator, with its disc type geometry, is conducive to easier integration with the turbine of the prime mover for both high- and low-speed applications, when compared with its radial flux counterpart.

Coreless axial flux permanent magnet (AFPM) machines have been extensively studied because of additional advantages of their enlarged air gap leading to low synchronous reactance, cogging torque free, high power factor and higher efficiency as a result of absence of core losses in the stator [2]. On the other hand, more PM material is used compared with iron-cored machines, and there might be notable eddy current losses in the stator windings that are directly exposed to magnetic field. However, the losses can be minimised by employing proper coil conductors like Litz wire so that the machine efficiency can be improved. A plastic structure multi-disc coreless AFPM motor is proposed to directly drive the propeller of the stratospheric unmanned aircraft because of its high efficiency over a wide power range and impressively light weight [3–5]. An AFPM motor with coreless stator and Halbach-magnet-array rotors without back irons is designed to drive a solar-powered electric vehicle at a hyper efficiency of 97.5% at rated power output and extremely high-power density [6]. Coreless AFPM machines are also eligible contenders for various power generation applications particularly in direct-drives over a wide operational speed range. For instance, coreless AFPM machines are investigated for low-speed applications for direct-coupled wind turbine generators [7–9], medium-speed applications for automotive generators [10–12] and in high-speed direct-coupled gas turbine generators for aerospace applications [13–17]. However, research on high-speed AFPM machines in low-cost man-portable power platform is relatively recent [18–19].

In this paper, a high-speed three-phase 1 kW coreless surface mounted AFPM generator with circular magnets and coils is proposed and studied. Both analytical and three-dimensional electromagnetic finite element analysis (3D FEA) models are employed to calculate the parameters

of the machine, and to further analyse and optimise the machine performance. Moreover, aluminium alloy holders are designed to withstand the considerable centrifugal forces acting on the magnets at high rotational speed. Finally, a prototype is designed and built for experimental tests and to demonstrate a relatively simple-to-manufacture structure using low-cost non-ferromagnetic aluminium alloy holders. Both the experimental and FEA results are in close agreements, which confirm the distinctive advantages of high-power density and efficiency of the proposed machine. In conclusion, the utility and challenges of this type of high-speed coreless AFPM generators are highlighted.

2 Machine structure and analytical modelling

Owing to their ease of fabrication and assembly, circular PMs and concentrated armature coils are employed to generate nearly sinusoidal voltage output [7]. Fig. 1 shows the 3D schematic structure of the high-speed coreless surface mounted AFPM generator under study, which consists of two rotor discs and one stator disc sandwiched in between. There is sufficient running mechanical clearance between the rotor and stator disc. As shown, circular axially magnetised high strength neodymium–iron–boron PMs (NdFe35) are circumferentially glued on the surface of the mild steel back iron with even space for each rotor disc. The magnets on each rotor disc are directly aligned and faced with the opposite polarity in the final assembly. Magnet holders made of non-ferromagnetic high-strength aluminium alloy are employed to fix and secure the PMs at high rotational speed. The three-phase concentrated circular armature coils are arranged circumferentially and potted by the non-ferromagnetic and non-conductive epoxy resin to form an integrated stator disc. It can be seen that the winding coils are directly exposed to high frequency magnetic field in the air gap because of the spinning rotors, which might introduce significant eddy current losses in the conductors. Consequently, fine multi-stranded insulated small wires are necessary to minimise the eddy current losses in the stator. Similar machine topologies are introduced as a low-speed small-scale wind turbine direct-drive generator [7] and a modified structure design for an automotive application [12], with an assumption that at the axial middle of the stator the flux density distribution induced by PMs takes the form of 'sinusoidal hills' with radii half of the rotor pole pitch. The peak flux density at the axial middle of the stator can be derived analytically with a reasonable accuracy as [7]

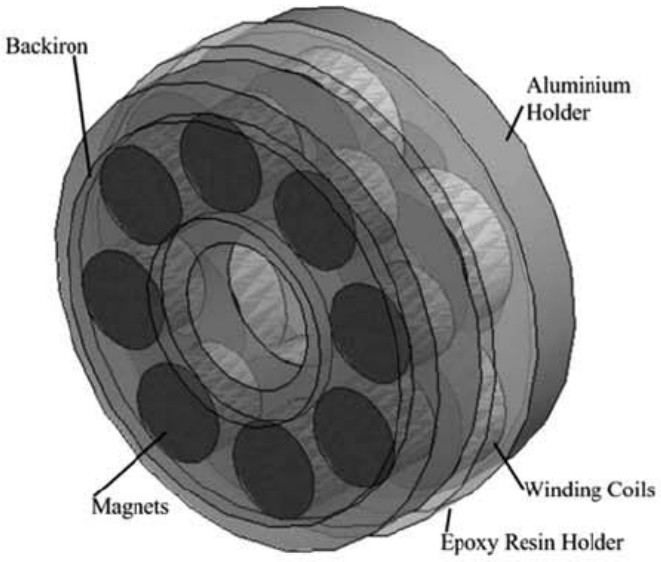

Figure 1 *Proposed machine structure*

$$B_{\text{peak}} = \frac{4B_{\text{r}}}{\pi\mu_{\text{r}}} \frac{\sin\left((pR_{\text{m}}/2R_{\text{c}})\right)\sinh\left((pl_{\text{m}}/2R_{\text{c}})\right)}{\sinh\left((p(2l_{\text{m}}+g))/4R_{\text{c}}\right)} \tag{1}$$

where B_{r} and μ_{r} are the magnet residual flux density and relative recoil permeability, respectively; R_{m} and R_{c} are radii of the circular magnets and the circle where the magnets are placed, respectively; l_{m} and g are the axial lengths of the magnets and active air gap, respectively; and p is the magnet pole number. Then the fundamental (rms) of the induced EMF in each armature coil can be calculated based on the first harmonic of the flux density only as

$$E_{\text{coil}} = \frac{\sqrt{2}\,k_1 k_2 n N_{\text{coil}} \pi^2 B_{\text{peak}} R_{\text{c}}^2}{15p^2(R_{\text{o}}-R_{\text{i}})}\left[4R_{\text{c}}\left(\sin\frac{pR_{\text{o}}}{2R_{\text{c}}}-\sin\frac{pR_{\text{i}}}{2R_{\text{c}}}\right)\right.$$
$$\left.-pR_{\text{o}}\left(1+\cos\frac{pR_{\text{o}}}{2R_{\text{c}}}\right)+pR_{\text{i}}\left(1+\cos\frac{pR_{\text{i}}}{2R_{\text{c}}}\right)\right] \tag{2}$$

where k_1 and k_2 are the corresponding flux enhancement factors to compensate the flux density in the radial direction that is not exactly sinusoidal distribution and the flux density in the axial direction that is not exactly same as the one in the axial middle of stator, which normally has a value slightly bigger than unity ($k_1 = 1.1$ and $k_2 = 1.05$ used in this paper), n is the rotational speed of the machine in revolution per minute (rpm), N_{coil} is the number of turns of each coil, R_{i} and R_{o} are circular winding coil inner and outer radii, respectively.

Moreover, an assumption that at the axial middle of the stator the flux density distribution generated by armature coils with current excitations follows 'conical' shapes has been taken in [7]. Therefore the flux density is presumed to be constant over the centre of the circular coil and to decrease linearly across the coil. However, substantial leakage fluxes around the coils because of the relative large equivalent air gap can be detected, which can be accounted for by using a leakage flux compensation factor $k_{\text{L}} = 1.5$. Consequently, the coil inductance can be evaluated by

$$L_{\text{coil}} = \frac{k_{\text{L}}\mu_0\pi N_{\text{coil}}^2}{6(g+2l_{\text{m}})}(R_{\text{o}}^2 + 2R_{\text{o}}R_{\text{i}} + 3R_{\text{i}}^2) \tag{3}$$

where μ_0 is the vacuum permeability. Since the proposed machine has a relatively high excitation frequency of 1.33 kHz, small multi-stranded copper wires are employed

to mitigate both skin and proximity effects. By excluding these effects, the coil resistance only depends on the winding package factor and coil inner and outer radii (R_i, R_o), as well as operating temperature, and it can be derived as

$$R_{coil} = \frac{\rho_{cu}\pi N_{coil}^2(R_o + R_i)(1 + k_{cu}(T - 20))}{k_p(g - 2c)(R_o - R_i)} \quad (4)$$

where T is the average temperature of the coil, k_{cu} is the average temperature coefficient of the copper resistivity, ρ_{cu} is the electric resistivity of the copper at 20°C temperature, k_p is the winding package factor and c is the running clearance between stator and rotor.

Neglecting the weak mutual effect between the coils, the values of stator phase EMF, inductance and resistance can be obtained as

$$E_{ph} = \frac{N_{s\_ph}}{N_{coil}}E_{coil}, \quad L_{ph} = \frac{N_{s\_ph}}{N_{coil}}L_{coil}, \quad R_{ph} = \frac{N_{s\_ph}}{N_{coil}}R_{coil} \quad (5)$$

where E_{ph}, R_{ph}, L_{ph} and N_{s_ph} are the EMF, resistance, inductance values per phase and the number of turns of windings in series each phase, respectively.

Fig. 2 shows the schematic circuit of the generator output is rectified and then loaded through a resistor, together with the equivalent one. The equivalent circuit parameters can be calculated as [7]

$$E_{dc} = \frac{3\sqrt{6}}{\pi}E_{ph}, \quad R_{dc} \simeq 2R_{ph}, \quad R_{overlap} = \frac{pn}{20}L_{ph} \quad (6)$$

By taking into account the voltage drops of the diodes, the direct current (DC) power output of the generator with rectifier can be easily assessed by analytically resolving the equivalent circuit at certain copper losses as

$$P_{dc} = \sqrt{\frac{(E_{dc} - V_{diode})^2 P_{cu}}{R_{overlap} + R_{dc}}} - P_{cu} \quad (7)$$

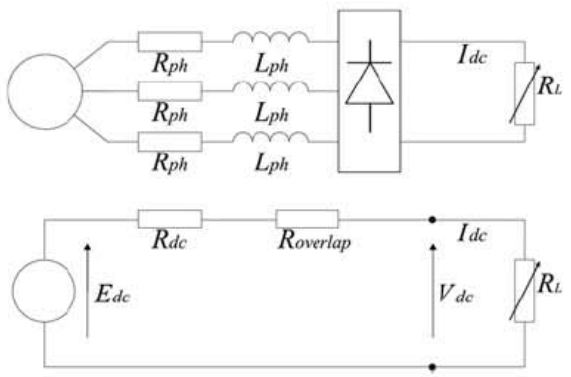

Figure 2 *DC resistive load circuit and the equivalent circuit*

where P_{cu} and V_{diode} are the stator copper losses and voltage drop in the diodes, respectively. Eddy currents are induced in the stator windings which are directly exposed to the magnetic field generated by PMs. However, it is quite difficult to estimate them accurately and efficiently, yet an FE-aided analytical model is presented and detailed in [20] to predict the eddy current losses accurately. In this study, eddy current losses are negligible as the small multi-stranded wires employed insignificant armature reaction because of the large air gap and negligible armature MMF harmonics owing to the nearly sinusoidal currents. Thus, the corresponding efficiency can be estimated as

$$\eta = \frac{E_{dc} - V_{diode}}{E_{dc}} - \frac{\sqrt{(R_{dc} + R_{overlap})P_{cu}}}{E_{dc}} \quad (8)$$

Moreover, there are considerable mechanical friction losses such as windage losses and bearing losses as a result of high rotational speed. Approximate analytical approaches are introduced in [16, 17], yet it is very difficult to predict them in reasonable accuracy. Generally, the rotor diameter should be as small as possible so as to attenuate the windage losses.

3 Machine design and FE validation

Small magnet poles such as two-pole or four-pole are normally considered for high-speed applications so that the electrical frequency can be minimised to improve the machine efficiency. In this study, because of their poor magnet and space utilisations, the machines with small magnet poles would exhibit much bigger machine diameters compared with the higher pole machines with same power output. Thus, it is necessary to consider a higher pole number configuration, which would however increase eddy current losses and assembly complexity. An eight-pole configuration has been chosen to offer better magnet utilisation with a small rotor diameter, which is critical for mechanical integrity at high speed. Forthwith, six concentrated circular coils are used for the eight-pole machine in order to achieve high winding space and factor, hence good performance [3, 7, 16]. Moreover, with the use of small multi-stranded wires to minimise eddy current losses, only a low winding package factor of 0.3 is achieved. Based on the analytical equations, a 1 kW generator at rated speed 20 000 rpm is sized and designed with off-the-shelf circular magnets in order to minimise the prototype cost. The key parameters of the machine are shown in Table 1.

On the other hand, AFPM machines are generally modelled in a 3D FEA because of its 3D flux distribution. To minimise extensive computational time, only quarter of the machine with periodic and symmetric boundary conditions is modelled. Fig. 3 shows the meshed model of quarter of the machine and Fig. 4 shows the magnetic flux

Table 1 Key design parameters of the machine

Symbol	Parameters	Values
P_{DC}	DC power output	1000 W
N	rated rotational speed	20 000 rpm
R_c	magnet placement circle radius	25 mm
B_r	magnet residual flux density	1.21 T
μ_r	magnet relative recoil permeability	1.1
P	magnet pole number	8
p_s	stator coil number	6
R_m	magnet radius	8 mm
l_m	magnet axial length	10 mm
G	air gap axial length	12 mm
C	running clearance	1 mm
l_b	back iron thickness	3 mm
L	machine total axial length	60 mm
R	machine radius	50 mm
k_p	winding package factor	30%
V_{diode}	diode voltage drop	1 V

Figure 3 *Meshed model of quarter of the machine*

density distribution in the machine with no load condition. Since the EMF and inductance of the coil can be computed accurately by the 3D FEA model, machine performance prediction and design optimisation can be achieved with confidence.

Since six concentrated coils are employed, the outer radius of the coil R_o can be directly calculated as 12.5 mm. The DC power outputs of the generator with varying winding coil inner radius R_i are evaluated by analytical and FEA models. The copper Joule losses P_{cu} are fixed as 100 W and the diode voltage drop is neglected during the whole

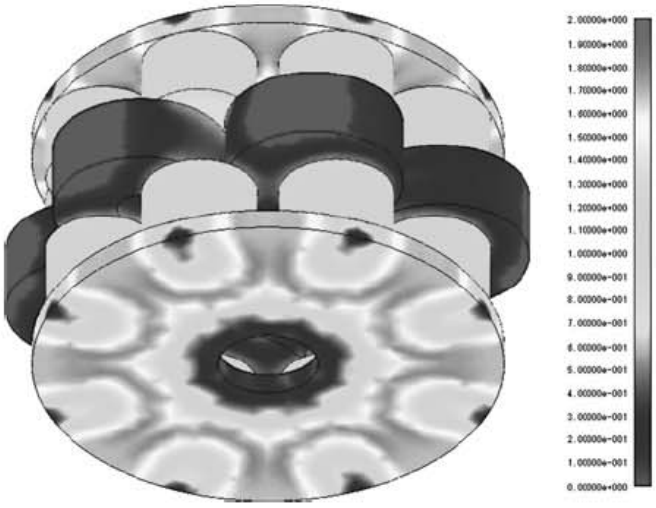

Figure 4 *No-load magnetic flux density distribution in the machine*

analysis. The predicted DC power outputs, and EMF and inductance errors, between the analytical and FEA results are illustrated as Figs. 5 and 6, respectively. It can be seen that the analytical DC power outputs are getting gradually smaller than the FEA ones along when R_i is increasing in Fig. 5, which can be explained by EMF errors between in Fig. 6. Consequently, bigger flux enhancement factor k_1 is

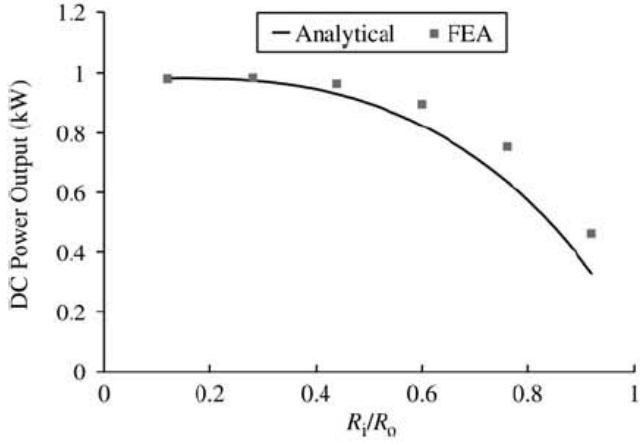

Figure 5 *DC power output against coil inner radius between FEA and analytical results*

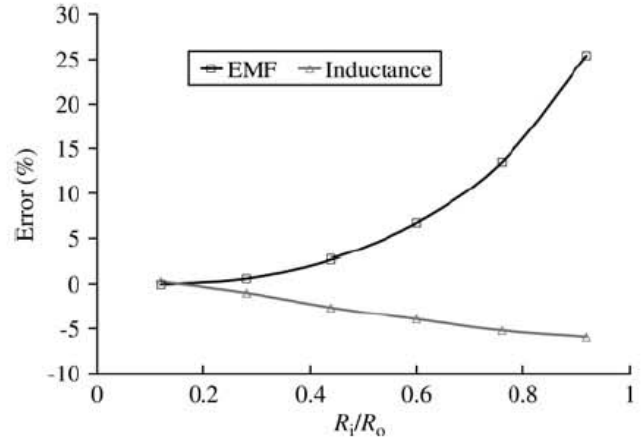

Figure 6 *EMF and inductance errors between FEA and analytical results*

highly desirable for the accurate prediction of the machine performance, because of the stronger impact of the non-sinusoidal radial components for bigger R_i. It also can be inspected from Fig. 6 that the inductance errors between are much stable and smaller than the EMF ones. It can be concluded that the flux enhancement factor k_1 should be carefully determined according to the relative values of R_o and R_i, in order to achieve accurate analytical predictions. Meanwhile, it is noted that the DC power output of the machine will first gradually increase first and then decrease as R_i is getting bigger, and the machine with optimal $R_i = 3.5$ mm could deliver nearly 1 kW DC power. The analytical and FEA results are in reasonable agreements, especially for small R_i, thus the analytical equations are verified for preliminary machine design.

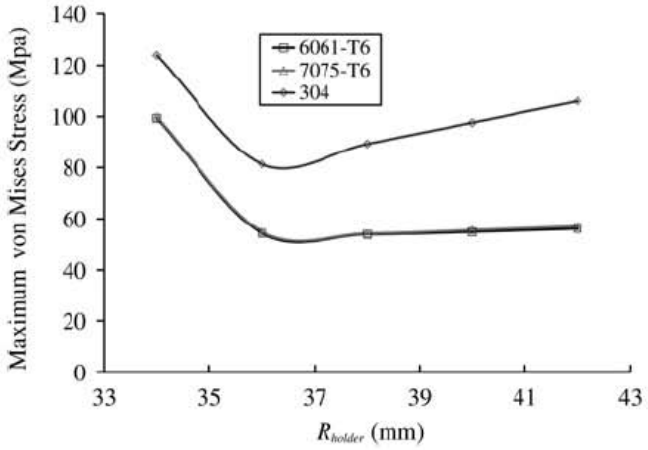

Figure 7 *Maximum von Mises stress against holder radius at 20 000 rpm*

4 Mechanical holder design

High centrifugal forces will be exerted on the PMs when the machine is operated at relatively high speed, therefore non-ferromagnetic high strength holders are required to hold the magnets against high centrifugal force and to ensure rotor integrity. Mechanical design of the magnet holder turns into one of the key issues for the proposed machine.

In this study, three common non-ferromagnetic materials, aluminium alloy 6061-T6, 7075-T6 and stainless steel 304, are considered for the magnet holder, and Table 2 shows the mechanical property of the materials. The mechanical stresses induced in the rotor discs are estimated using 3D FEA software, ANSYS 11.0. As a starting point, the mechanical stress distributions in different rotor discs with different materials and radii are calculated at 20 000 rpm, and the maximum von Mises stresses are illustrated in Fig. 7. It can be seen that the stainless steel holder exhibits higher stress than the aluminium alloy ones because of its higher density and for all the materials the stress first decreases and then increases when the magnet holder radius R_{holder} increases, which implies that the impact of centrifugal forces on the magnets are mostly cancelled out by the holder after R_{holder} reaches around 37 mm for the proposed machine. Consequently, the magnet holder radius of 40 mm has been chosen, allowing for a safety margin. Subsequently, the mechanical stress distributions in the rotor discs with different materials and same R_{holder} of 40 mm are calculated at different speed, and the maximum von Mises stresses are depicted in Fig. 8, which apparently shows that the maximum safe operational speed is less than 30 000 rpm for a stainless steel holder, more than 40 000 rpm for aluminium alloy 6061-T6 and more than 50 000 rpm for aluminium allay 7075-T6. Considering the cost and weight of the machine, aluminium alloy 6061-T6, which is sufficient enough for the proposed machine, is employed for the prototype. Finally, Fig. 9 shows the estimated von Mises stress distribution of the final rotor disc at 20 000 rpm with shaft shrink fit consideration. It can be seen that the high stress is concentrated nearby the shaft because of the effect of shrink fit. Ignoring the stress concentration, the maximum stress in the holder is about 120 MPa, which is much less than the allowable stress for aluminium alloy 6061-T6, as well as in the shaft. On the other hand, the stresses in the magnets are much smaller, and far less than the compressive strength of NdFe35. The results of the mechanical analysis assure the mechanical integrity of rotor using aluminium alloy 6061-T6.

Table 2 Mechanical property of the material

Material	Young's modulus, GPa	Density, kg/m^3	Poisson's ratio	Allowable stress, MPa
7075-T6	71.4	2810	0.33	434–476
6061-T6	73	2700	0.33	241
NdFe35	160	7500	0.24	140 (1000)[a]
304	197	7930	0.29	205

[a]Tensile strength and compressive strength

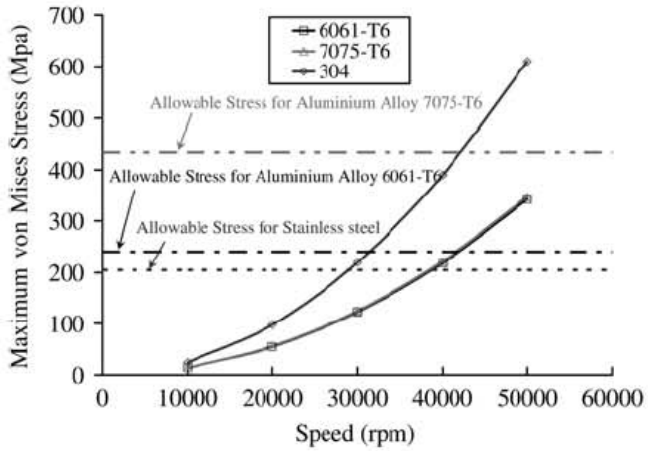

Figure 8 *Maximum von Mises stress against speed for 40 mm holder radius*

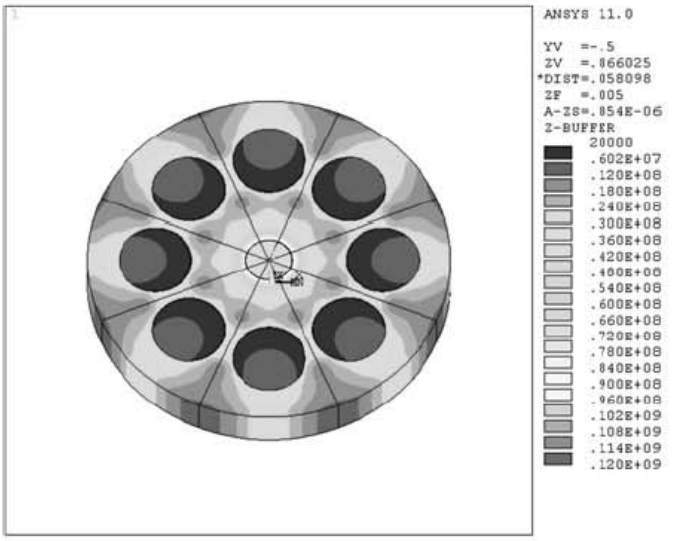

Figure 9 *von Mises stress distribution of the proposed rotor disc*

5 Prototype and experimental validation

Based on the aforementioned design data, a prototype generator has been fabricated for testing. Each coil in stator has 82 turns of 26-stranded wires of 0.12 mm diameter, and the two armature coils in each phase are connected in series. The magnets with aluminium alloy holder (rotor disc), coiled in epoxy resin (stator disk) and assembled machine are shown in Fig. 10. The machine resistance and inductance are measured at room temperature and compared with those calculated from the analytical and 3D FEA models. The measured and predicted values are given in Table 3, which show good agreements among the results. The resistance differences among the measured results are attributed to broken strand wires in phase *b* during the assembly of the machine.

Fig. 11 shows the experimental setup for testing, where the prototype generator is primed moved by a high-speed PM brushless motor, and is loaded with resistance via a simple standard six-pulse rectifier with filter capacitor connected. Owing to the safety procedure imposed in laboratory environments, the prototype has been tested up to half of the rated speed. The line EMF profiles at 10 000 rpm and their harmonic analysis from analytical equations (fundamental component), 3D FEA model and experiment are compared in Fig. 12 and Table 4, respectively, which show good agreements between the 3D FEA and measured ones as well as the analytical one. Moreover, the line EMF is essentially sinusoidal with negligible total harmonic distortion.

The output of the prototype is rectified for performance testing. Experimental tests have been undertaken at 10 000 rpm with currents between 0 and 8 A. The rectified DC voltage against load DC at different speed is first measured and shown in Fig. 13 together with evaluated one, and Fig. 14 shows the predicted and experimental DC

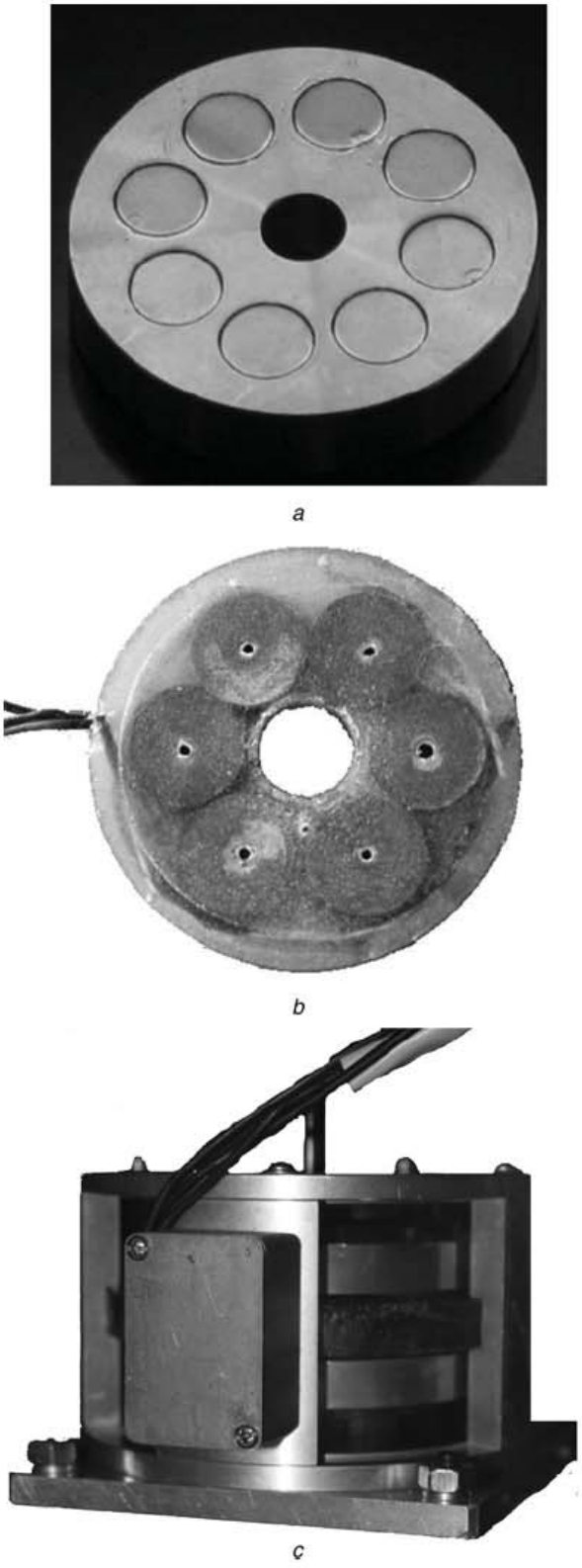

a

b

c

Figure 10 *Prototype machine*

a Rotor disc
b Stator disc
c Assembled machine

power output from the rectifier. Again, excellent agreements between the predicted and measured results are evident. The DC output efficiency of the prototype has been measured and is shown in Fig. 15. Fig. 16 shows the rectifier output voltage and current waveforms when the prototype is driven at 10 000 rpm with nearly 500 W power output. The prototype enjoys nearly 85% efficiency at 500 W DC power output from the test. It is envisaged

Table 3 Prototype resistance and inductance

Parameters	Analytical	3D FEA	Measured
R_{ab}, Ω	0.983	~	0.818
R_{ac}, Ω	0.983	~	0.781
R_{bc}, Ω	0.983	~	0.819
L_{ab}, μH	232.7	216.5	227.6
L_{ac}, μH	232.7	216.5	232.3
L_{bc}, μH	232.7	216.5	240.0

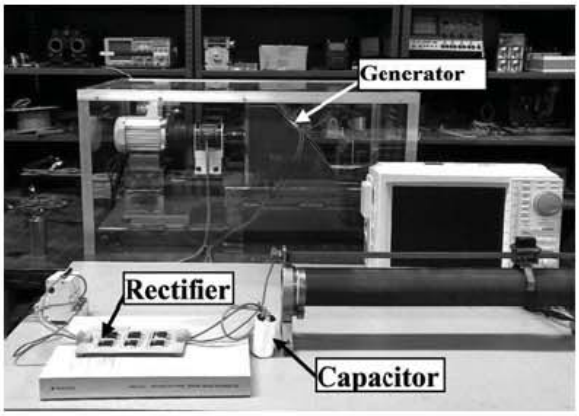

Figure 11 *Experiment setup*

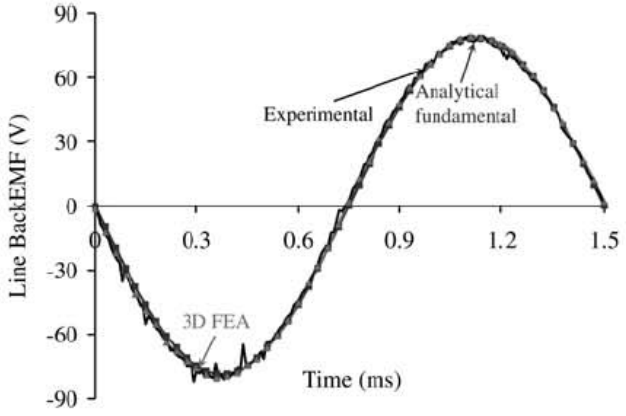

Figure 12 *Comparison of line EMF waveforms at 10 000 rpm*

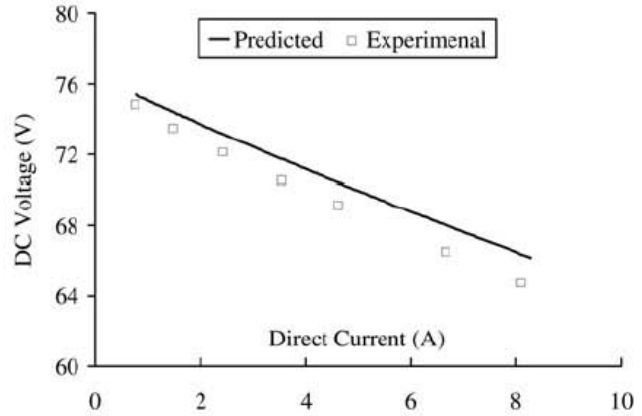

Figure 13 *Predicted and experimental DC output voltage against DC load current at 10 000 rpm*

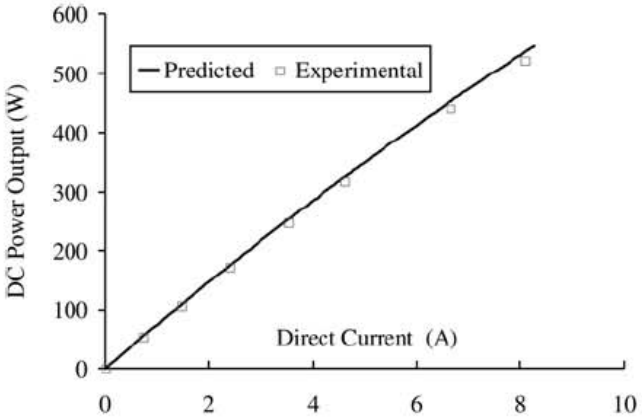

Figure 14 *Predicted and experimental DC power output against DC current at 10 000 rpm*

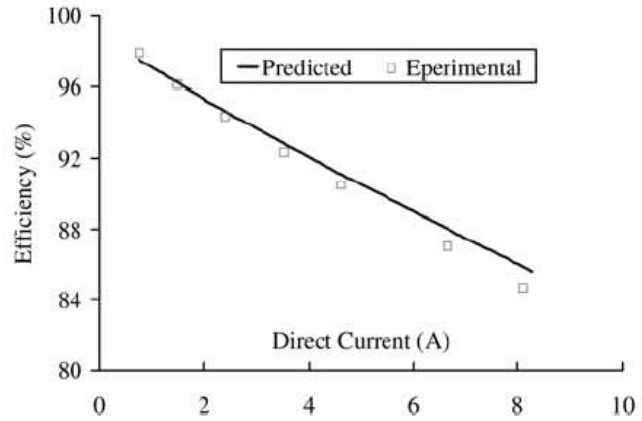

Figure 15 *Predicted and experimental efficiency against DC current at 10 000 rpm*

Table 4 Harmonic analysis of line EMF

Harmonics	1ST	5TH	7th	11th	13th	17th	19th
analytical, V	78.7	~	~	~	~	~	~
3D FEA, V	79.9	0.562	0.363	0.0832	0.309	0.161	0.151
experimental, V	79.0	0.241	0.356	0.112	0.303	0.424	0.305

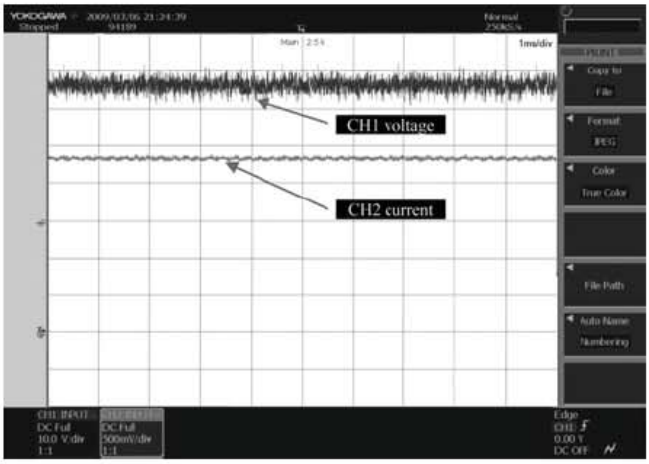

Figure 16 *Rectifier DC voltage and current waveforms at 10 000 rpm*

(CH1: DC voltage 65 V, CH2: DC 800 mv, 100 mv = 1 A)

that the prototype will also be capable of delivering 1 kW DC power at 20 000 rpm with similar high efficiency.

6 Conclusions

This paper presents a comprehensive design and performance analysis of a high-speed coreless low-power AFPM generator. Approximate analytical equations are derived for preliminary design and a 1 kW prototype machine is sized using off-the-shelf PMs. Then, the 3D FEA model is developed to validate the analytical model, and to optimise the design of machine coil. The mechanical stress and integrity analysis of the rotor and magnet holder at high rotational speed are also given.

Finally, a prototype machine has been fabricated for validation purposes. Comprehensive tests on the machine have been undertaken with DC-resistive load using standard six-pulse rectifier. The experimental results demonstrate excellent agreements with the predicted ones. The prototype has been extensively tested at up to 50% rated load and operational speed because of the laboratory regulations and experimental limitations. The results overwhelmingly show that the proposed machine is a highly compact and efficient generator with very simple and robust structure that can be manufactured and assembled at extremely low cost with off-the-shelf magnets.

Acknowledgments

This work was funded by Direct Research and Consultancy, Ref: RACR/041/06, DCMT, Defence Academy, UK. The authors are also deeply grateful to Powersys for providing the finite element software JMAG-Studio 9.0 for this work and Mr. Chen Yuan from Wujiang Nanyuan Electrical Co., Ltd., People's Republic of China for the prototype generator fabrications.

References

[1] MINISTRY OF DEFENCE, UK: 'Future protected vehicle capability vision CDE call v1.0' (Ministry of Defence, June 2009)

[2] GIERAS J.F., WANG R.J., KAMPER M.J.: 'Axial flux permanent magnet brushless machines' (Springer, 2008, 2nd edn.)

[3] HILL-COTTINGHAM R.J., COLES P.C., EASTHAM J.F., PROFUMO F., TENCONI A., GIANOLIO G.: 'Multi-disc axial flux stratospheric aircraft propeller drive'. Proc. 36th IEEE Industry Applications Conf., October 2001, pp. 1634–1639

[4] HILL-COTTINGHAM R.J., COLES P.C., EASTHAM J.F., PROFUMO F., TENCONI A., GIANOLIO G.: 'Novel axial flux machine for aircraft drive: design and modeling', *IEEE Trans. Magn.*, 2002, **38**, (5), pp. 3003–3005

[5] HILL-COTTINGHAM R.J., COLES P.C., EASTHAM J.F., PROFUMO F., TENCONI A., GIANOLIO G.: 'A plastic structure multi-disc axial flux PM motor'. Proc. 37th IEEE Industry Applications Conf., October 2002, pp. 1274–1280

[6] LOVATT H.C., RAMSDEN V.S., MECROW B.C.: 'Design of an in-wheel motor for a solar-powered electric vehicle', *Proc. Inst. Electr. Eng. Electr. Power Appl.*, 1998, **145**, (5), pp. 402–408

[7] BUMBY J.R., MARTIN R.: 'Axial-flux permanent-magnet air-cored generator for small-scale wind turbines', *Proc. Inst. Electr. Eng. Electr. Power Appl.*, 2005, **152**, (5), pp. 1065–1075

[8] CHAN T.F., LAI L.L.: 'An axial flux permanent-magnet synchronous generator for a direct-coupled wind-turbine system', *IEEE Trans. Energy Convers.*, 2007, **22**, (1), pp. 86–94

[9] KAMPER M.J., WANG R.J., ROSSOUW F.G.: 'Analysis and performance of axial flux permanent-magnet machine with air-cored nonoverlapping concentrated stator windings', *IEEE Trans. Ind. Appl.*, 2008, **44**, (5), pp. 1495–1504

[10] WANG R.J., KAMPER M.J., WESTHUIZEN K.V., GIERAS J.F.: 'Optimal design of a coreless stator axial flux permanent-magnet generator', *IEEE Trans. Magn.*, 2005, **41**, (1), pp. 55–64

[11] HOSSEINI S.M., AGHA-MIRSALIM M., MIRZAEI M.: 'Design, prototyping, and analysis of a low cost axial-flux coreless permanent-magnet generator', *IEEE Trans. Magn.*, 2008, **44**, (1), pp. 75–80

[12] JAVADI S., MIRSALIM M.: 'A coreless axial-flux permanent-magnet generator for automotive applications', *IEEE Trans. Magn.*, 2008, **44**, (12), pp. 4591–4598

[13] PULLEN K.R., ETEMAD M.R., FENOCCHI A.: 'The high speed axial flux disc generator-unlocking the potential of the automotive gas turbine'. Proc. IEE Colloquium on Machines and Drives for Electric and Hybrid Vehicles, 1996, pp. 8/1–8/4

[14] EL-HASAN T.S., LUK P.C.K., BHINDER F.S., EBAID M.S.: 'Modular design of high-speed permanent-magnet axial flux generator', *IEEE Trans. Magn.*, 2000, **36**, (5), pp. 3558–3561

[15] EL-HASAN T.S., LUK P.C.K.: 'Magnet topology optimization to reduce harmonics in high speed axial flux generators', *IEEE Trans. Magn.*, 2003, **39**, (5), pp. 3340–3342

[16] FEI W., LUK P.C.K.: 'Design of a 1 kW high speed axial flux permanent-magnet machine'. Proc. IET Power Electronics, Machines and Drives Conf., 2008, pp. 230–234

[17] SADEGHIERAD M., LESANI H., MONSEF H., DARABI A.: 'Design considerations of high speed axial flux permanent magnet generator with coreless stator'. Proc. Int. Power Engineering Conf., 2007, pp. 1097–1102

[18] FEI W., LUK P.C.K.: 'Design and performance analysis of a high-speed air-cored axial-flux permanent-magnet generator with circular magnets and coils'. Proc. IEEE Int. Electrical Machines and Drives Conf., May 2009, pp. 1617–1624

[19] SADEGHIERAD M., DARABI A., LESANI H., MONSEF H.: 'Rotor yoke thickness of coreless high-speed axial-flux permanent magnet generator', *IEEE Trans. Magn.*, 2009, **45**, (4), pp. 2032–2037

[20] WANG R.J., KAMPER M.J.: 'Calculation of eddy current loss in axial field permanent-magnet machine with coreless stator', *IEEE Trans. Energy Convers.*, 2004, **19**, (3), pp. 532–538